Superconductor Science and Technology

PAPER

Synthesis routes to eliminate oxide impurity segregation and their influence on intergrain connectivity in K-doped $BaFe_2As_2$ polycrystalline bulks

To cite this article: C Pak *et al* 2020 *Supercond. Sci. Technol.* **33** 084010

IOP Publishing Superconductor Science and Technology
Supercond. Sci. Technol. **33** (2020) 084010 (9pp) https://doi.org/10.1088/1361-6668/aba01a

Synthesis routes to eliminate oxide impurity segregation and their influence on intergrain connectivity in K-doped $BaFe_2As_2$ polycrystalline bulks

C Pak[1], Y F Su[1], Y Collantes[1], C Tarantini[1], E E Hellstrom[1,2], D C Larbalestier[1,2] and F Kametani[1,2]

[1] Applied Superconductivity Center, National High Magnetic Field Laboratory, Tallahassee, FL 32310, United States of America
[2] Department of Mechanical Engineering, Florida State University, Tallahassee, FL 32310, United States of America

E-mail: kametani@asc.magnet.fsu.edu

Received 30 March 2020, revised 14 June 2020
Accepted for publication 25 June 2020
Published 13 July 2020

Abstract

The poor reproducibility of intergrain critical current density J_c in Fe-based superconductors is often believed to result from uncontrolled grain boundary (GB) connectivity degraded by extrinsic factors such as the local or global impurity concentration or GB porosity or cracks. Earlier we found that Ba and K can appear as oxide impurities at GBs, along with GB-wetting FeAs. In this study, we evaluated how the sample preparation environment and purity of the starting materials influence the polycrystalline J_c in K-doped $BaFe_2As_2$ (Ba122) bulks. Using a high-performance glovebox, the oxygen and water levels were significantly reduced, eliminating traces of FeAs. Oxide impurities and Ba (or K) segregation associated with oxygen in the starting materials were significantly reduced by using high purity starting materials. This combination essentially doubled the best J_c*(4.2 K)* values to 2.3×10^5 at self-field and 1.6×10^4 A cm^{-2} at 10 T and analytical scanning transmission electron microscopy showed no GB or O segregation in the best samples, but did show dark Z-contrast and distinct nanoscale porosity. Our work shows that an inert synthesis environment and high purity K and Ba do reduce current-blocking oxygen impurity and GB impurity phases, allowing deeper exploration of the role of extrinsic and intrinsic GB blocking effects in controlling the J_c of polycrystalline Ba122.

Keywords: iron-based, Bulk superconductor, synthesis, superconducting properties

(Some figures may appear in colour only in the online journal)

1. Introduction

For high field applications, there are two vital superconducting requirements, a high critical current density (J_c) and a high upper critical field (H_{c2}). A high critical temperature (T_c) and low superconducting anisotropy are also highly desirable. The strong demand to pursue high-field magnets beyond the H_{c2} limits of low temperature superconductors (LTS) drives extensive research and development of high temperature superconductor cuprates including BSCCO [$Bi_2Sr_2CaCu_2O_x$ (Bi-2212), $Bi_2Sr_2Ca_2Cu_3O_x$ (Bi-2223)], and REBCO ($REBa_2Cu_3O_x$), because they possess high T_c and H_{c2} [1–3]. One major technological challenge of HTS cuprates is their high anisotropy in conductor form (REBCO and Bi-2223), while another is their high conductor cost (REBCO, Bi-2223 and Bi-2212). Fe-based

superconductors (FBS), which are the newest members of the high-field superconductor family, have the potential to be used for high-field applications above 16 T due to their relatively high critical temperature, low H_{c2} anisotropy, and high H_{c2} [4–9]. K-doped $BaFe_2As_2$ (K-Ba122) possesses a T_c of 38 K at optimum stoichiometry $Ba_{0.6}K_{0.4}Fe_2As_2$, and H_{c2} of ~90 T [10–12]. Moreover, all of the elemental components in K-Ba122 are earth-abundant compared to other HTS materials, potentially contributing to a favorable cost benefit if high J_c K-Ba122 wires can be realized [10, 13–17].

Practical applications of high temperature superconductors usually demand long length wires in which the superconductor is polycrystalline. The exception is REBCO, which is a quasi-single crystal in long-length coated conductor geometry [18–21]. The key property that needs to be demonstrated for K-Ba122 is high J_c in polycrystalline, preferably untextured, forms that would allow round wires [10]. So far, however, single crystals of K-Ba122 have much higher J_c than polycrystalline wires or tapes, suggesting degraded connectivity, particularly at grain boundaries [10, 18, 22–24]. Improving the connectivity between grains is key to making J_c of the Fe-based superconductors competitive against present day LTS and HTS conductors. There are two possible factors that can degrade the intergrain connectivity. One is intrinsic associated with the basic physics of GB disorder arising from the short coherence length, low carrier density, and local suppression of the superconducting order parameter [22, 25]. The second kind are extrinsic factors such as GB composition fluctuations and segregation of impurities, such as oxygen, that have also been reported to degrade J_c [26, 27]. Systematic bicrystal experiments that created artificial, straight [001] tilt GBs in Co-doped Ba122 suggested that GBs with high misorientation angle act as intrinsic weak links, although perhaps less strongly than in the HTS cuprates [25, 27]. However, previous studies also suggested that the grain connectivity in FBS compounds including Ba122 can be easily degraded by extrinsic factors such as local or global impurity concentrations and GB cracks and voids [11, 26, 28–30]. The unpredictable GB connectivity caused by such extrinsic factors often results in poor reproducibility of intergrain J_c [24]. Indeed our early analytical microscopy studies revealed that Ba and K, as well as oxide impurities can all segregate to the GBs in the final bulks. However, it was not clear whether the oxide impurities in our K-Ba122 polycrystals came from the starting materials or formed during the synthesis process.

In this study, we extensively investigated the synthesis environment, especially the oxygen and moisture level inside the glovebox and the purity of starting materials. By revisiting and modifying our earlier synthesis route [11], we were able to eliminate the GB segregation of Ba or K and/or their oxide impurities and also prevent FeAs formation. We found that a dry and oxygen-free environment is critical not only for maintaining the quality of the starting materials but also for preventing segregation of oxide impurities to the GBs during synthesis. We found that high-purity K and Ba improve the homogeneity of K-Ba122 and significantly decrease oxide impurities, resulting in higher J_c that we attribute to better intergrain connectivity.

2. Experimental procedures

Polycrystalline $Ba_{0.6}K_{0.4}Fe_2As_2$ bulks were synthesized from elemental starting materials. We used elemental Ba and K with two different purities: regular purity Ba of $\geqslant$99.2% and high purity Ba of $\geqslant$99.9% purity. We used the highest purity, commercially available Fe and As (Fe $\geqslant$99.99% and As $\geqslant$99.99999%) as received. We mixed the elements in the stoichiometric ratio of $Ba_{0.6}K_{0.4}Fe_2As_2$ with 10 mol. % additional K (thus the nominal starting composition is $Ba_{0.6}K_{0.44}Fe_2As_2$), weighing them out and placing them into the milling jar in one of the two Ar-filled gloveboxes. Excess K is expected to compensate for the possible loss of K during the synthesis so that we can complete the reaction to form K-doped Ba122 The mixtures, sealed in their milling jars were removed from the glovebox, to then thoroughly mix and grind them in a Fritsch P7 Premium planetary ball-mill for one hour. After milling, the milling jar was returned to the glovebox, and the powder loaded into a niobium (Nb) crucible, which was itself loaded into a steel crucible that was then evacuated, and welded shut. The sealed steel crucible was compressed by cold isostatic pressing (CIP) at 276 MPa and then heat treated by hot isostatic pressing (HIP) at 9.7 MPa at varying temperatures between 600 and 825 °C for 20 h. After this first heat treatment, the sample was again thoroughly ground using the same milling process, packed in Nb and stainless steel, evacuated and welded shut, CIPped, and then heat treated by HIP for 10 h at 193 MPa and 600 °C. All of the chemical handling procedures were carried out exclusively inside one of the two argon-filled gloveboxes. We used a high-performance glove box in which the O_2 and H_2O level were maintained at $\leqslant$0.005 ppm and $\leqslant$0.06 ppm, respectively. For comparison, we also prepared a sample in the regular glovebox used in all our earlier syntheses in which the O_2 and H_2O levels were as high as 100 ppm and 10 ppm, respectively. Table 1 lists the sample names, the glovebox used, the K and Ba purity, the first heat treatment (HT) temperature, and electromagnetic properties of the samples. Note that the second heat treatment was identical for all samples (10 h HIP at 193 MPa at 600 °C).

Room temperature powder x-ray diffraction (PXRD) was performed on a Panalytical X'pert Pro diffractometer equipped with an X'Celerator detector with a CuK_α radiation source ($\lambda = 1.54187$ Å). The HighScore Plus [31] and FullProf [32] software packages were used for global phase identification, profile fitting, and unit cell refinement.

Magnetic property measurements were carried out on slab-shaped samples cut and polished from the polycrystalline bulks using a Quantum Design SQUID magnetometer MPMS XL5. Zero field cooled temperature dependent magnetization was measured from 5 to 50 K with a heating rate of 0.2 K min^{-1} and 2 mT magnetic field applied parallel to the long sample edge. The field-dependent magnetization (−2 to 14 T) was measured at 4.2 K using an Oxford Instruments 14 T Vibrating Sample Magnetometer (VSM). The magnetization J_c was calculated based on the Bean model using the nominal sample size around ~3.5 × 1.0 × 0.4 mm^3, where dimensions were defined by careful cutting and polishing of each sample. For calculating J_c, the supercurrent was assumed to

Table 1. List of samples that were prepared with different gloveboxes, different purity of Ba and K, and different heat treatments, plus electromagnetic properties of these samples. J_c was measured at 4.2 K.

Sample	Glovebox	K purity	Ba Purity	1st HT Temp. (°C)	T_{c_onset} (K)	$J_{c\_0\ T}$ (A cm^{-2})	$J_{c\_10\ T}$ (A cm^{-2})
A- R	Regular	Regular	Regular	600	35	8.52×10^4	5.71×10^3
A- HP	High Performance	Regular	Regular	600	35	1.10×10^5	6.92×10^3
B	High Performance	High	Regular	600	31.8	1.02×10^5	7.72×10^3
C	High Performance	High	Regular	675	32.6	1.63×10^5	1.30×10^4
D	High Performance	High	Regular	750	31.8	1.49×10^5	9.94×10^3
E	High Performance	High	High	600	33.1	1.22×10^5	1.08×10^4
F	High Performance	High	High	675	34.5	1.45×10^5	1.24×10^4
G	High Performance	High	High	750	34.8	2.33×10^5	1.61×10^4
H	High Performance	High	High	825	33.5	1.54×10^4	1.15×10^4

circulate over the whole sample, although we do recognize as discussed later that current loops may exist on multiple, smaller scales too [33, 34]. (Scanning) transmission electron microscope (S/TEM) imaging and elemental analysis were performed in a probe-corrected JEOL JEM-ARM200cF with an Oxford X-Max^N 100TLE SDD energy dispersive x-ray spectroscopy (EDS) detector.

Table 1 tabulates the sample name, the type of glove box, HT variables and the resulting T_{c_onset} and J_c. We note that while the first heat treatment temperature varied from 600 °C to 825 °C, all other heat treatment parameters (ramping rate, temperature, pressure, and duration), including the second heat treatment were the same.

3. Results

Figure 1 shows the PXRD patterns of the samples made in the high-performance glovebox (Samples B to H in table 1). Thanks to the 10 mol% excess K, all samples are quite phase-pure with no noticeable trace of 2nd phase FeAs. Judged by the PXRD patterns in figure 1, there is no distinguishable difference in phase purity among our samples, although they may contain slightly different amounts of oxide impurity phases that cannot be detected by PXRD.

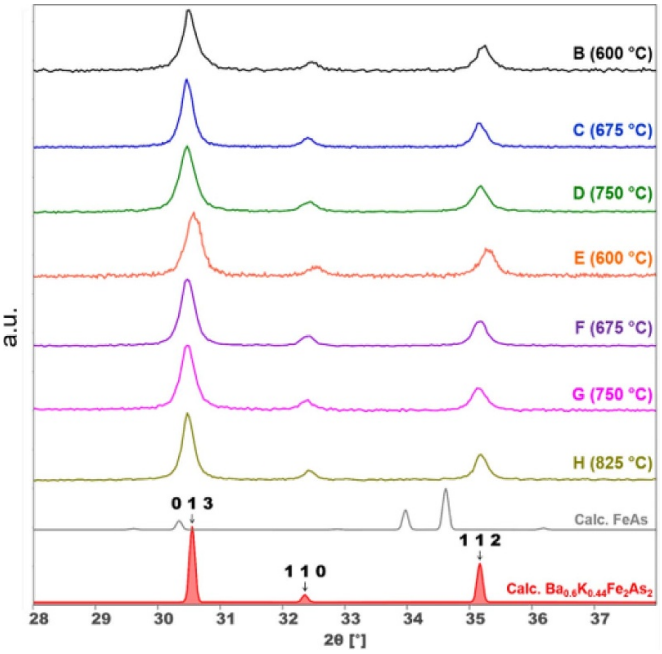

Figure 1. Powder x-ray diffraction patterns of samples B-H with nominal composition $Ba_{0.6}K_{0.44}Fe_2As_2$ that had different first heat treatment temperatures.

Figure 2 compares the temperature-dependent T_c transition curves. All samples show 3 ~ 6 K lower T_{c_onset} than reported for the 38 K of optimally doped K-Ba122 single crystals [9]. As shown in figure 2(a), the glovebox slightly affects the T_c. Samples A-R (prepared in the regular glovebox with regular purity K and Ba) and A-HP (prepared in the high-performance glovebox with regular purity K and Ba) have their T_c onset at 35 K. Higher K purity reduced T_c to 31.8 K when the high-performance glove box was used (Sample B on figure 2(b)). Figure 2(b) also shows that T_c is not very sensitive to the 1st HT temperature. When high purity Ba and high purity K are used (samples F-H), T_c is the same as for sample A-HP as shown in figure 2(c). Samples F-H (1st HT temperature is 675 °C, 750 °C, 825 °C, respectively) show a T_c onset of about 34.3 K, although T_c of Sample E (1st HT at 600 °C) is slightly lower, ~33.5 K.

As shown in figure 3(a), sample A-R (prepared in the regular glovebox using regular purity elements) exhibits J_c of ~9.0×10^4 A cm^{-2} at self-field, decreasing rather quickly at low fields and reaching ~6×10^3 A cm^{-2} at 10 T. Sample A-HP, prepared in the high performance glovebox, exhibits a slightly improved J_c of ~1.0×10^5 A cm^{-2} at self-field and ~7.0×10^3 A cm^{-2} at 10 T; however, as seen in figure 3(a), J_c still decays quickly at low fields. As shown in figure 3(b), J_c increases with high purity K. J_c at self-field increases to ~1.5×10^5 A cm^{-2} for sample C and D after a 1st HT at 675 °C and 750 °C, respectively. As shown in figure 3(c), the highest J_c was obtained when both high purity K and Ba were used. Sample G, processed at 750 °C during the 1st HT, shows a J_c of ~2.3×10^5 A cm^{-2} (SF) and ~1.6×10^4 A cm^{-2} at 10 T. It is important to note that the field dependence of J_c at low-field is less pronounced with higher purity K and Ba, as shown in samples B-D and E-H (figures 3(b) and (c)).

The 4.2 K field dependent pinning force $F_P(H)$ is shown in figure 4. Both samples A-R and A-HP (figure 4(a)) show an unusual kink at around 1 T followed by an almost linear rise from 2 to 10 T. Smoother F_P(H) plots and higher values of

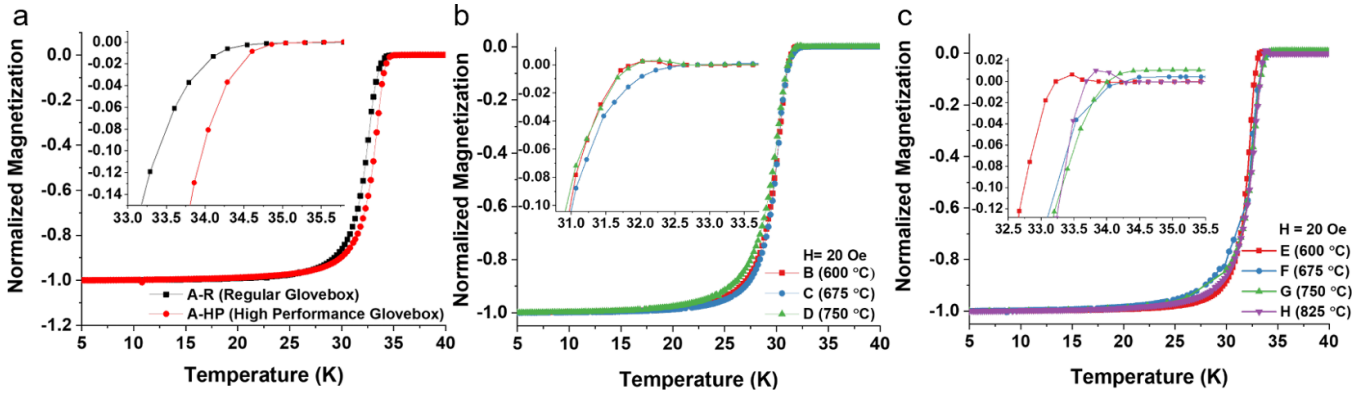

Figure 2. Normalized zero-field cooling temperature dependent magnetization heated from 5 K in an applied field of 2 mT on samples synthesized with (a) regular or high performance glovebox with regular Ba and K (samples A-R and A-HP), (b) high performance glovebox with regular Ba and high purity K (samples B—D), and (c) high performance glovebox with high purity Ba, K (samples E—G).

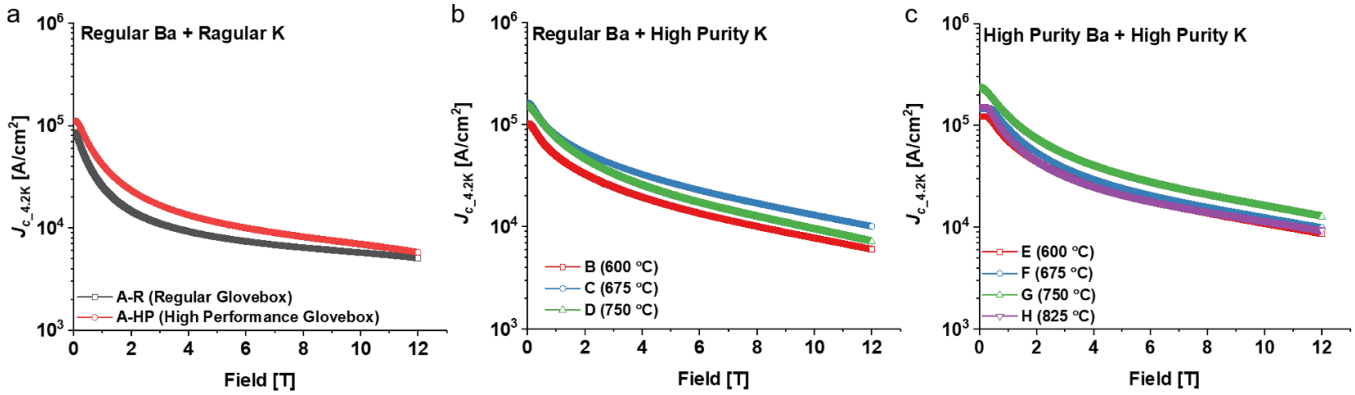

Figure 3. J_c(H) plots for $Ba_{0.6}K_{0.4}Fe_2As_2$ with regular high purity Ba prepared in the regular or the high-performance glovebox.

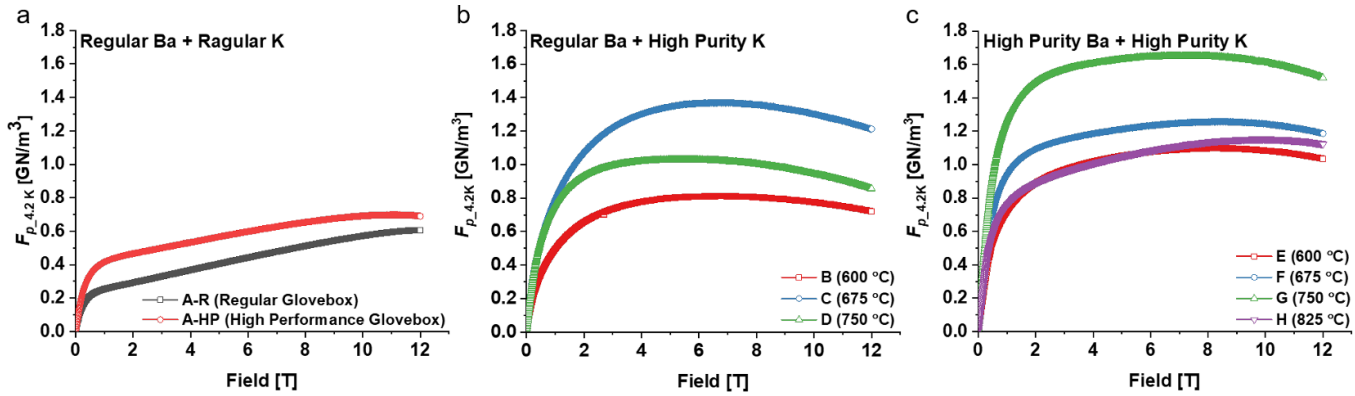

Figure 4. Field dependent flux pinning force plots for $Ba_{0.6}K_{0.44}Fe_2As_2$ (nominal) with regular Ba or high purity Ba prepared in regular or high performance glovebox.

F_P(H) were seen for samples made with higher purity K, the highest values being for samples made with both high purity K and Ba, as is seen in figure 4(c) (sample E, F, G, and H). Sample G, processed at 750 °C during the 1st HT, shows an F_p maximum of ~1.6 GN m^{-3}, almost three times larger than Sample A-R made with regular purity elements in the regular glove box.

S/TEM imaging was performed on samples A-R, A-HP, D, and G. Figure 5(a) shows a representative microstructure of sample A-R made with regular purity elements in the regular glovebox, which is also representative of the grain size and the 2nd phase impurities before we decreased the oxygen and water content in the glovebox. The average grain size is ~50 nm and there are a significant number of large FeAs grains and an amorphous Ba-O phase that preferentially appears at the grain boundaries. In sample A-HP (high performance glovebox with regular Ba and K), K-Ba122 grains appear better connected compared to sample A-R, judged by

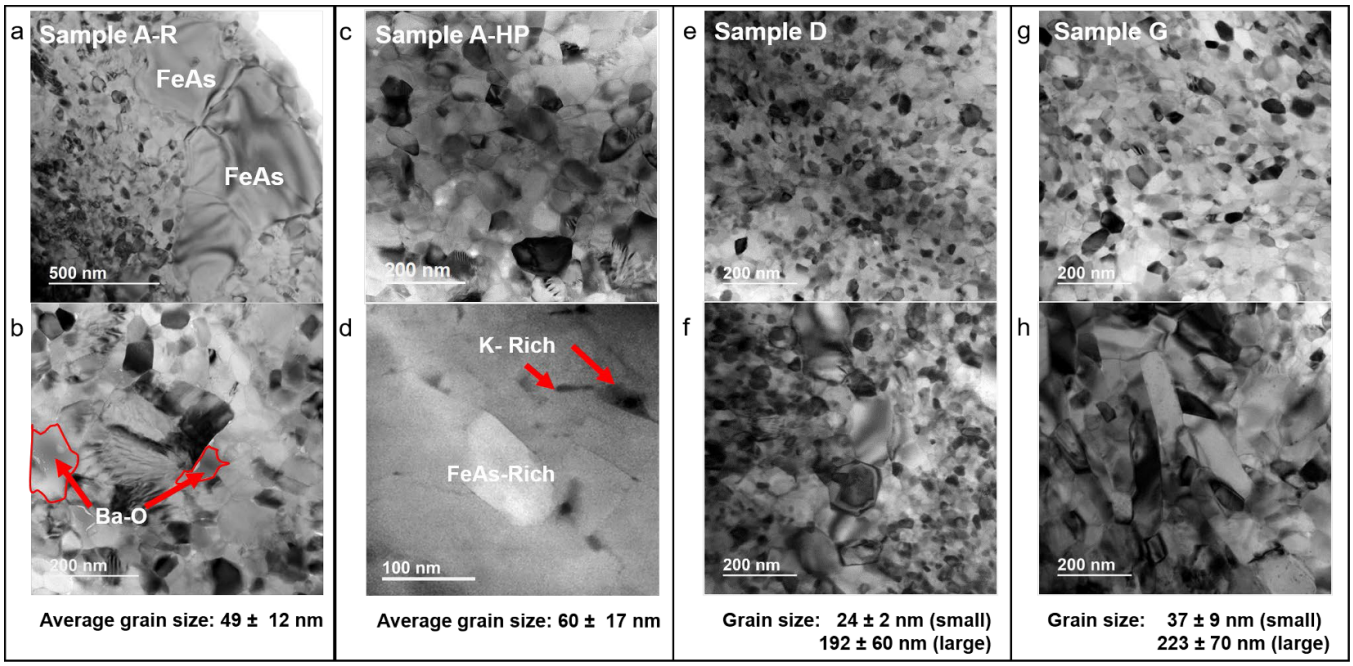

Figure 5. Representative grain structures in (a) and (b) sample A-R; (c) and (d) sample A-HP; (e) and (f) sample D; and (g) and (h) sample G. The bright field TEM images show diffraction contrast within each $Ba_{0.6}K_{0.4}Fe_2As_2$ grain and FeAs phase. The high angle annular dark field STEM image of g shows the FeAs and K-rich grain boundaries in sample A-HP.

the absence of amorphous GB Ba-O trace (figure 5(b)) and the average grain size is ~10 nm larger than A-R. However, there are still FeAs-rich areas and K segregation observed at the grain boundaries (figure 5(d)), and also intergrain connectivity is not sufficiently good. By increasing the purity of K and Ba (sample D: figures 5(e) and (f); sample G: figures 5(g) and (h)), GB K segregation is significantly suppressed as well as FeAs and Ba-O. The average grain size also decreased in sample D (high purity K + regular Ba) and G (high purity K + Ba). Interestingly both D and G showed a bimodal grain size distribution, although the large grain regions were rather minor (~5% of the volume fraction) in both samples. The average grain size in the fine grain regions in samples D and G is ~24 nm and ~37 nm, respectively (figures 5(e) and (g)). In the large grain regions, the grain size is approximately 190 nm in sample D and ~220 nm in sample G. The large grains in sample G shows a plate-like rather than the equiaxed shape that is seen in sample D.

The high angle annular dark field scanning electron microscopy (HAADF-STEM) image in figure 6(a), shows a dark Z-contrast at many GBs in sample G, indicating a low atomic density. This indicates either local GB porosity or light element segregation and/or oxide impurities at the GB, in either case suggesting compromised superconducting connectivity. However, the EDS line scan across the GB (figure 6(b)) does not show any increase of oxygen or noticeable variation in composition, suggesting that this dark GB Z-contrast is primarily caused by nanoscale cracks or porosity along the GBs.

EDS analysis of individual grains in samples D and G was performed. We calculated the chemical composition of our samples by normalizing to the sum of Ba and K concentration. The average composition of sample D is $Ba_{0.58}K_{0.42}Fe_{1.92}As_{2.08}$ regardless of grain size. The average compositions of small and large grains are slightly different in sample G, $Ba_{0.62}K_{0.38}Fe_{2.11}As_{2.06}$ in large grains and $Ba_{0.59}K_{0.41}Fe_{1.85}As_{2.70}$ in small grains with an overall composition of $Ba_{0.61}K_{0.39}Fe_2As_{2.36}$ which is slightly As-rich. We do not fully understand the slight excess of As in the small grains. Since the TEM sample thickness is larger than the average small grain size in this sample, the EDS analysis possibly captures some minor compositional variation at the grain boundaries and/or amorphous layer at the TEM specimen surface.

4. Discussion

4.1. Synthesis conditions and their outcomes

Our results show that high purity K and Ba and a very clean glove box do improve the reaction completeness of K-Ba122 as judged by the lack of FeAs in fully reacted samples D and G. We reason that small traces of O_2 or H_2O tie up K and/or Ba as K-O and/or Ba-O impurities, making the reaction to form K-Ba122 incomplete and leaving undesired FeAs, often found as a GB phase, in the final product (sample A-R). We also consider the possibility that the K and/or Ba compositions will be under-estimated if impure, surface-contaminated Ba or K starting material is used. In addition, regular purity Ba and K are normally immersed in mineral oil, which must be carefully removed, and their surfaces scraped to remove surface oxides. Consistent with this reasoning, the microscopy in figure 5 shows that samples made with regular purity Ba and K have residual FeAs (samples A-R and A-HP). By contrast, the high purity elements come in sealed ampoules under

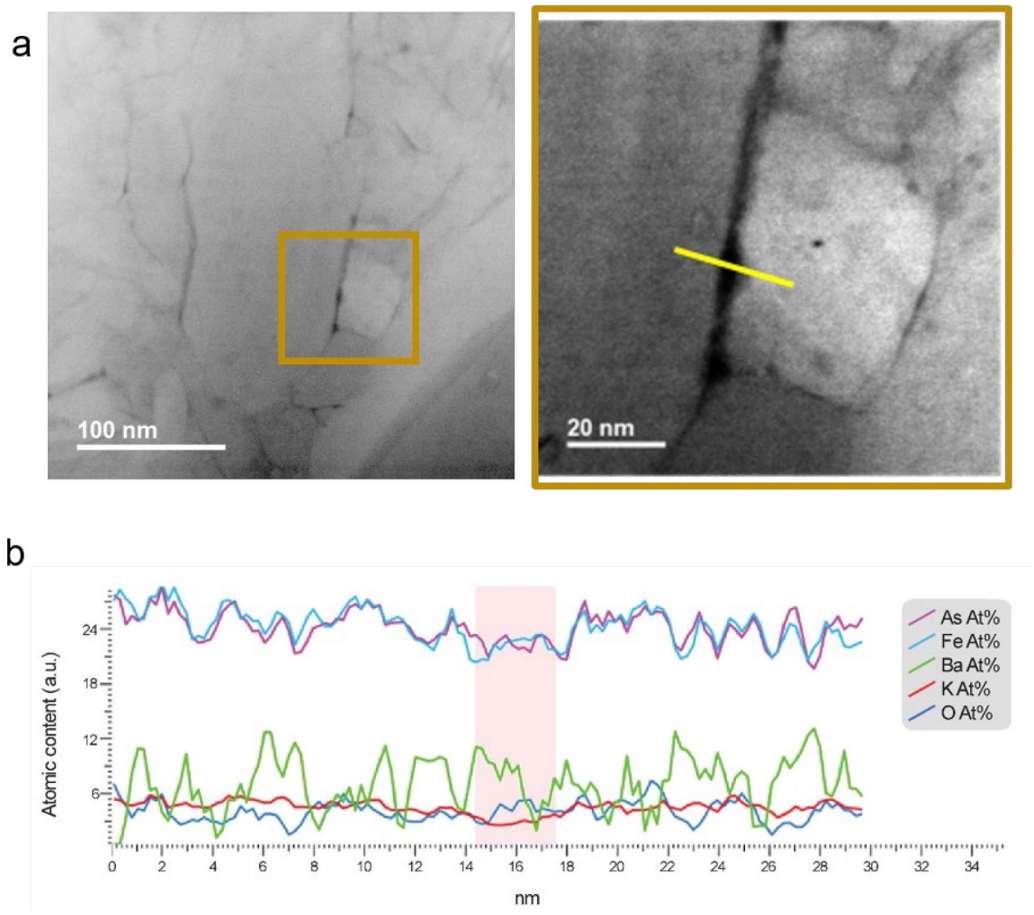

Figure 6. (a) High angle annular dark field scanning TEM image of representative GB in sample G. (b) EDS line scan across the grain boundary. The EDS scan was performed along the yellow line in (a).

argon, suggesting that there is no increase in O_2 and H_2O levels in the high-performance glovebox when the ampoule is opened, allowing immediate use without any further cleaning.

The significant reduction of O_2 and H_2O levels inside the high-performance glovebox (O_2: $\leqslant$0.005 ppm; H_2O: $\leqslant$0.06 ppm) reduces contamination of the air- and moisture-sensitive Ba and K and lessens the formation of oxide impurities in the final samples. Contaminants are also reduced because the milling jar is filled in the high-performance glovebox atmosphere. The gas-tight seals on the milling jar prevent any air entry during the milling step outside the glovebox.

4.2. Critical current density properties

By combining the high performance glovebox and high purity K and Ba, the J_c in the low field regime significantly improves, compared to regular purity samples A-R and A-HP (figure 3). The less rapid low-field J_c decay in high-purity samples B to H indicates that the intergrain connectivity is enhanced. The 10% excess of high purity K in the higher purity samples allows the reaction to go to completion, significantly suppressing the formation of FeAs and oxide impurities that we estimate were the central cause of the poorer intergrain connectivity in the samples of Weiss *et al* [11, 25]. Between the 600 °C samples, the difference in self-field J_c between A-R and A-HP is about 30% and the difference between B and E is about 20%; globally from A-R to E the self-field J_c increase is about 43%, so the increase is not negligible (see table 1). Moreover the in-field enhancement has to be considered as well: at 10 T, from A-R to A-HP the J_c enhancement is +21%, from A-HP to B is +11%, from B to E is +40% and, globally, from A-R to E is +89%. Those results clearly indicate the progressive improvement generated by the cleaner processing: although the high-performance glove box has a positive effect, using clear raw materials further improves the properties. It is interesting to note that the increase of J_c at 10 T is twice as large as at self-field. This suggests that improving the grain boundary cleanness does not simply improve the connectivity, but also enhances the pinning efficiency.

In the case of the 1st HT at 750 °C, by using high purity Ba and high purity K (sample G), J_c further improved by 56% at self-field and 62% at 10 T compared to samples with regular Ba and high purity K (sample D). Figure 7 shows J_c of samples with different purities of Ba and K as a function of the 1st HT temperature, emphasizing that the highest J_c was indeed achieved for 750 °C 1st HT temperature for sample G with high purity Ba and K. It appears that temperatures >600 °C for the 1st HT are not as detrimental as was initially found by Weiss *et al* [30].

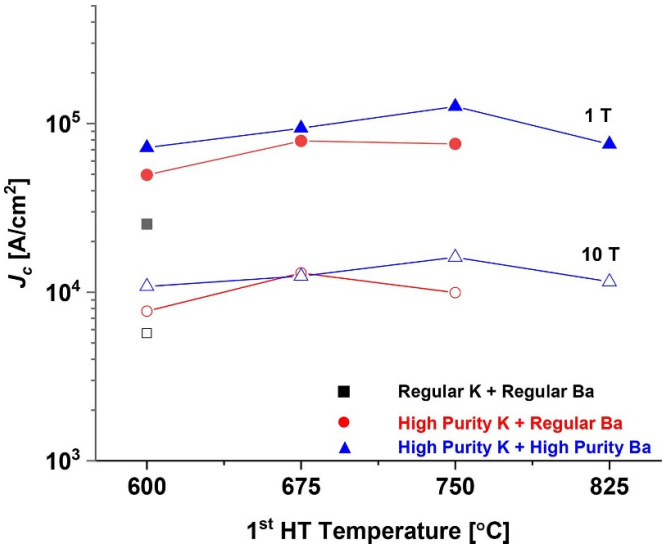

Figure 7. Effect of high purity starting materials on critical current density measured at 4.2 K. Solid points are measured at 1 T, and hallow points are measured at 10 T.

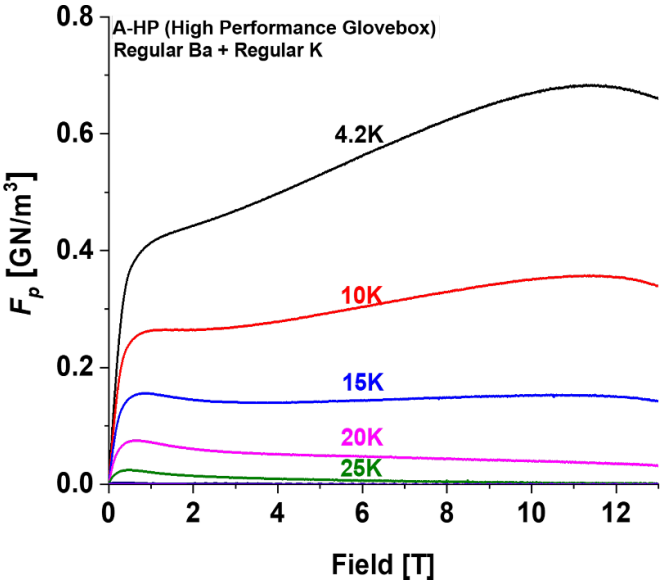

Figure 8. Field dependence of the pinning force of sample A-HP at different temperatures.

The differences between samples of varying purity and 1st HT temperature becomes more apparent in the linear F_P(H) plots than in the logarithmic $J_c(H)$ plots. The initial steep linear rise in F_p observed in samples A-R and A-HP in figure 4(a) is unusual, as is an inflection at such a low field (<1 T). Indeed, this inflection is seen in figure 8 up to at least 20 K in sample A-HP, even as the higher field behaviour shows much more sensitivity to field and temperature. This type of anomalies is not common in bulk samples but can be seen in films with artificially introduced pinning centres as for instance reported in ref. 35 and 36 work done by Tarantini *et. al.* and Opherden *et. al.*, respectively [35, 36]. In the case of samples A-R and A-HP, we believe that this F_p anomaly may be determined by a matching between the fine grains whose GBs contain FeAs or BaO and the vortex spacing. In fact the average 60 nm grain size of sample A-HP corresponds to a matching field of ~0.6 T, compatible with the inflection position observed in figure 8. The implication of such matching is that the impurity in the GB (figures 5(c) and (d)) is enhancing the vortex pinning, enforcing strong GB vortex pinning at all temperatures. Sadly, these phases also reduce the connectivity, thus lowering the measured J_c defined by using the whole cross-section as the area normalization. In the high purity samples (e.g. D and G) with higher J_c, there is no F_p inflection anomaly, consistent with their higher J_c being due to better intergrain connectivity, even if there are still poorly connected GBs as shown by figure 6.

4.3. Superconducting transition temperature properties

A striking result is that none, not even the high purity samples, achieved the expected 38 K T_c of single crystals, even though the transitions in figure 2 are all sharp, even for the least pure A-R sample. The T_c in fact does not show systematic dependence on starting-element purity or glovebox. Indeed, the high performance glovebox samples often (but not always) had T_c 0.7–2.5 K lower compared to samples prepared in the regular glovebox. One possibility is that their very small grain size (~20–40 nm) induces sufficient lattice strain to significantly distort the Fe-As bond angles, thus degrading T_c [37, 38]. Indeed, by our TEM analysis, we found the overall grain sizes (A-R, A-HP, D, G) are much smaller than those observed by other groups [15, 39]. The ultra-fine grain size may have its origin in the high-energy ball milling step prior to the second HT. We believe that it amorphizes the crystalline K-Ba122 phase formed in the first HT [40, 41]. Samples D (regular purity Ba and high purity K) and sample G (high purity Ba and K) were both given a 2nd HT at 750 °C and both showed a bimodal grain size, sample G having the highest T_c of 34.8 K. However, sample D had nearly the lowest T_c of 31.8 K, making it clear that multiple variables are simultaneously in play.

Nevertheless the grain size of all samples measured in our study are about one order of magnitude smaller than the London penetration depth λ of optimally doped Ba122, which is ~200–250 nm [42]. If all GBs in such small grain samples are weakly linked, the magnetic flux would preferentially penetrate every GB, making the T_c transition very broad. However, as shown in figure 2, all T_c transitions are quite sharp despite the very small grains, indicating that on average the connectivity at the majority of GBs is not compromised and superconducting shielding over a significant portion of the sample can be established. We also need to keep in mind that small contaminations at GBs embedded within the samples cannot be detected by low-field ZFC measurements, whereas they can effectively reduce the cross-section when the current is induced through the entire sample during hysteresis loop characterizations.

4.4. Length scales of current flow in the polycrystals

Judging from figures 3 and 4, the combination of high performance glovebox and pure Ba and K does improve the

intergrain J_c evaluated by considering that current flows over the whole sample. This does demonstrate the benefit of our high purity synthesis protocol. However, according to Ishida *et al*, the J_c(4.2 K) of 41% K-doped Ba122 crystals is ~1.0×10^6 A cm^{-2} and ~1.4×10^5 A cm^{-2} at self-field and 6 T, respectively [43], about 5 times that of our best J_c. This large J_c difference makes it logical to think that there are still many obstacles to current flow, especially at GBs. One residual obstacle is the porosity evident in figure 6. There remain still both extrinsic and intrinsic reasons for GBs to obstruct current flow. The sharp T_c transitions do suggest that the average GB is NOT a weak link, because smearing of the transition occurs on length scales of order 10λ (where λ is the London penetration depth), that is on a scale of order 2.5 μm, some thousand times the grain size. The sharp transitions mean that the shielding currents induced in the ZFC SQUID measurements (figure 2) must be at least on this scale. We conclude that the sharp transitions imply that, even if local GB contaminations affect the percolative connectivity of large ensembles of grains, domains of well-connected 20–40 nm grains form that are much larger than λ (=200–250 nm) with a strongly linked percolative current path within the domains. The overall low J_c compared to single crystals means that the overall connectivity of this complex network is still far from 100%.

The major unknown issue is still the degree to which the [001] tilt bicrystal experiments [22] explain that low J_c is now a problem intrinsic to weak-linking of high-angle GBs. Our experiments do now place some constraints on the value of high-pressure, high-purity synthesis. It is clear that we were able to raise J_c by effectively reducing the FeAs wetting phase, elemental segregation at the GBs, and macroscopic cracks and porosity. However, as figure 6 shows, the thin, dark Z-contrast at the GB indicates nanoscale cracks or porosity which still reduce the effective cross-section for supercurrent flow. We need to refine our synthesis to eliminate such low density GBs before we can conclude that we are at the intrinsic connectivity limit of intergranular transport.

5. Conclusions

We developed an effective synthesis route for making K-Ba122 bulks with minimal amounts of current-blocking impurities at the GBs by using a high-performance glove box and high purity Ba and K. Our systematic study of synthesis routes strongly suggests that high purity Ba and K and the first HT temperature are crucial to enhance the superconducting connectivity in the K-Ba122 polycrystals. This clean synthesis method significantly suppressed current-blocking FeAs and oxide GB by-products. The highest J_c (4.2 K) was 2.3×10^5 A cm^{-2} at self-field and 1.6×10^4 A cm^{-2} at 10 T, respectively. However, our best J_c is still only ~20% of single crystal J_c, strongly suggesting degraded polycrystalline connectivity remains at GB obstacles. TEM nanostructural analysis revealed that the poor intergrain connectivity in our samples is no longer caused by GB impurity segregation, but may be due to nanoscale GB porosity. Further optimization of grain size and densification needs to be done to evaluate residual intrinsic blocking effects of high angle GBs and assess how much further scope there is for processing improvements like this reported here to further improve the intergrain J_c of K-Ba122.

Acknowledgments

This work was supported by the US Department of Energy Office of High Energy Physics under the Grant Nos. DE-SC0018750, by the National High Magnetic Field Laboratory (which is supported by the National Science Foundation under NSF/DMR-1644779), and by the State of Florida.

ORCID iDs

C Pak https://orcid.org/0000-0002-9783-599X
C Tarantini https://orcid.org/0000-0002-3314-5906
E E Hellstrom https://orcid.org/0000-0001-8263-8662
D C Larbalestier https://orcid.org/0000-0001-7098-7208

References

[1] Campbell A M and Evetts J E 1972 *Adv. Phys.* **21** 199
[2] Matsumoto K, Nishihara M, Kimoto T, Horide T, Jha A K, Yoshida Y, Awaji S and Ichinose A 2017 *Supercond. Sci. Technol.* **30** 104006
[3] Saint-James D, Thomas E and Sarma G 1970 *Type II superconductivity* (Oxford: Pergamon)
[4] Fang L *et al* 2012 *Appl. Phys. Lett.* **101** 012601
[5] Kamihara Y, Watanabe T, Hirano M and Hosono H 2008 *J. Am. Chem. Soc.* **130** 3296
[6] Rotter M, Tegel M, Johrendt D, Schellenberg I, Hermes W and Pöttgen R 2008 *Phys. Rev.* B **78** 020503
[7] Wang X C, Liu Q Q, Lv Y X, Gao W B, Yang L X, Yu R C, Li F Y and Jin C Q 2008 *Solid State Commun.* **148** 538
[8] Tamegai T, Nakajima Y, Tsuchiya Y, Iyo A, Miyazawa K, M, Shirage P, Kito H and Eisaki H 2008 *J. Phys. Soc. Japan* **77** 54
[9] Rotter M, Tegel M and Johrendt D 2008 *Phys. Rev. Lett.* **101** 107006
[10] Larbalestier D, Gurevich A, Feldmann D M and Polyanskii A 2001 *Nature* **414** 368
[11] Weiss J D, Tarantini C, Jiang J, Kametani F, Polyanskii A A, Larbalestier D C and Hellstrom E E 2012 *Nat. Mater.* **11** 682
[12] Tarantini C, Gurevich A, Jaroszynski J, Balakirev F, Bellingeri E, Pallecchi I, Ferdeghini C, Shen B, Wen H H and Larbalestier D C 2011 *Phys. Rev.* B **84** 184522
[13] Pyon S, Suwa T, Park A, Kajitani H, Koizumi N, Tsuchiya Y, Awaji S, Watanabe K and Tamegai T 2016 *Supercond. Sci. Technol.* **29** 115002
[14] Pyon S, Suwa T, Tamegai T, Takano K, Kajitani H, Koizumi N, Awaji S, Zhou N and Shi Z 2018 *Supercond. Sci. Technol.* **31** 055016
[15] Huang H, Yao C, Dong C, Zhang X, Wang D, Cheng Z, Li J, Awaji S, Wen H and Ma Y 2017 *Supercond. Sci. Technol.* **31** 015017
[16] Lin H, Yao C, Zhang X, Zhang H, Wang D, Zhang Q, Ma Y, Awaji S and Watanabe K 2014 *Sci. Rep.* **4** 4465
[17] Gao Z, Togano K, Zhang Y, Matsumoto A, Kikuchi A and Kumakura H 2017 *Supercond. Sci. Technol.* **30** 095012
[18] Ding Q-P, Prombood T, Tsuchiya Y, Nakajima Y and Tamegai T 2012 *Supercond. Sci. Technol.* **25** 035019

[19] Ma Y, Gao Z, Qi Y, Zhang X, Wang L, Zhang Z and Wang D 2009 *Physica* C **469** 651
[20] Malagoli A, Wiesenmayer E, Marchner S, Johrendt D, Genovese A and Putti M 2015 *Supercond. Sci. Technol.* **28** 095015
[21] Togano K, Matsumoto A and Kumakura H 2010 *Supercond. Sci. Technol.* **23** 045009
[22] Durrell J H, Eom C B, Gurevich A, Hellstrom E E, Tarantini C, Yamamoto A and Larbalestier D C 2011 *Rep. Prog. Phys.* **74** 124511
[23] Hecher J, Baumgartner T, Weiss J D, Tarantini C, Yamamoto A, Jiang J, Hellstrom E E, Larbalestier D C and Eisterer M 2015 *Supercond. Sci. Technol.* **29** 025004
[24] Hosono H, Yamamoto A, Hiramatsu H and Ma Y 2018 *Mater. Today* **21** 278
[25] Lee S *et al* 2009 *Appl. Phys. Lett.* **95** 212505
[26] Kim Y-J, Weiss J D, Hellstrom E E, Larbalestier D C and Seidman D N 2014 *Appl. Phys. Lett.* **105** 162604
[27] Katase T, Ishimaru Y, Tsukamoto A, Hiramatsu H, Kamiya T, Tanabe K and Hosono H 2011 *Nat. Commun.* **2** 409
[28] Kametani F *et al* 2009 *Appl. Phys. Lett.* **95** 142502
[29] Nikolo M, Weiss J D, Singleton J, Jiang J and Hellstrom E E 2018 *IEEE Trans. Appl. Supercond.* **28** 1
[30] Weiss J D, Jiang J, Polyanskii A A and Hellstrom E E 2013 *Supercond. Sci. Technol.* **26** 074003
[31] Degen T, Sadki M, Bron E, König U, Nénert G 2014 *Powder Diffraction* **29** S13–S18
[32] Rodríguez-Carvajal J 1993 *Physica* B **192** 55
[33] Bean C P 1964 *Rev. Mod. Phys.* **36** 31
[34] Wang C, Gao Z, Yao C, Wang L, Qi Y, Wang D, Zhang X and Ma Y 2011 *Supercond. Sci. Technol.* **24** 065002
[35] Tarantini C, Lee S, Kametani F, Jiang J, Weiss J D, Jaroszynski J, Folkman C M, Hellstrom E E, Eom C B and Larbalestier D C 2012 *Phys. Rev.* B **86** 214504
[36] Opherden L *et al* 2016 *Sci. Rep.* **6** 21188
[37] Tokuta S and Yamamoto A 2019 *APL Mater.* **7** 111107
[38] Jing G, Qi W and Li-Ling S 2018 *Acta Phys. Sin.* **67** 207409
[39] Liu S, Lin K, Yao C, Zhang X, Dong C, Wang D, Awaji S, Kumakura H and Ma Y 2017 *Supercond. Sci. Technol.* **30** 115007
[40] Shimada Y, Yamamoto A, Hayashi Y, Kishio K, Shimoyama J-I, Hata S and Konno T J 2019 *Supercond. Sci. Technol.* **32** 084003
[41] Iida K, Hänisch J and Yamamoto A 2020 *Supercond. Sci. Technol.* **33** 043001
[42] Prozorov R and Kogan V G 2011 *Rep. Prog. Phys.* **74** 124505
[43] Ishida S, Song D, Ogino H, Iyo A, Eisaki H, Nakajima M, Shimoyama J-I and Eisterer M 2017 *Phys. Rev.* B **95** 014517